

A Resonantly Driven, Electroluminescent Metal Oxide Semiconductor Capacitor with High Power Efficiency

Vivian Wang and Ali Javey*



Cite This: <https://doi.org/10.1021/acsnano.1c05729>



Read Online

ACCESS |



Metrics & More



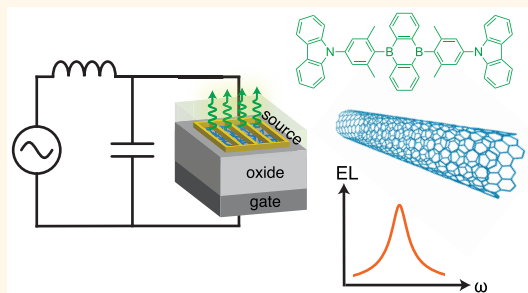
Article Recommendations



Supporting Information

ABSTRACT: Electroluminescence can be generated from a wide variety of emissive materials using a simple, generic device structure. In such a device, emissive materials are deposited by various means on a metal oxide semiconductor capacitor structure across which alternating current voltage is applied. However, these devices suffer from low external efficiencies and require the application of high voltages, thus hindering their practical usage and raising questions about the possible efficiencies that can be achieved using alternating current driving schemes in which injection of bipolar charges does not occur simultaneously. We show that appropriately chosen reactive electrical components can be leveraged to generate passive voltage gain across the device, allowing operation at input voltages below 1 V for devices across a range of gate oxide thicknesses. Furthermore, high power efficiencies are observed when using thermally activated delayed fluorescence emitters deposited by a single thermal evaporation step, suggesting that the efficiency of a light-emitting device with simplified structure can be high.

KEYWORDS: electroluminescence, alternating current, carbon nanotube, resonator, capacitor, light-emitting



Electroluminescent devices, which generate light emission in response to electrical excitation, have been extensively studied and developed since the early 1900s.¹ The phenomenon of electroluminescence (EL) was discovered in silicon carbide in 1907 and was later observed to occur in insulating materials containing zinc sulfide (ZnS) phosphor powder as well. The ZnS powder-based electroluminescent devices developed by Destriau in 1936 were operated by applying alternating current (AC) voltages.² Although this class of devices requires large voltages in the range of 100 V or more, they have found modern use in applications requiring simple and robust fabrication procedures, such as decorative electroluminescent wire,³ large-area textile displays,⁴ and sprayable interfaces.⁵ EL in organic materials was demonstrated in 1953 by Bernanose, who applied kilovolts of alternating voltage to fluorescent dyes like acridine orange.⁶ Since the initial demonstration of EL, a variety of light-emitting diodes (LEDs) based on inorganic and organic materials have been developed with ongoing improvements in brightness and efficiency over the past few decades.^{7–9} In these devices, electrons and holes are injected into an emissive layer by applying direct current (DC) voltage, often with the aid of multiple charge injection and transport layers surrounding the emissive layer.¹⁰

We have recently shown that EL can also be achieved from a variety of emissive materials at relatively low AC voltages (<100 V) using a metal oxide semiconductor (MOS) capacitor structure with a porous carbon nanotube (CNT) network as the top contact (Figure 1a).¹¹ These devices are compatible with emissive layers spanning a wide range of material classes (from colloidal quantum dots to small organic molecules to conjugated polymers and more), physical forms (from thin evaporated films to thick drop-casted films), and colors (across the entire visible range and beyond). The generic, open-top device structure enables facile integration of arbitrary emitters with applications in EL spectroscopy, light-emitting devices, and sensing. For inorganic semiconducting materials with sufficiently high carrier mobility such as transition metal dichalcogenide (TMDC) monolayers, applying AC voltage to MOS capacitors with top metal contacts alone is enough to generate EL.¹² However, visible EL cannot be obtained from

Received: July 6, 2021

Accepted: August 24, 2021

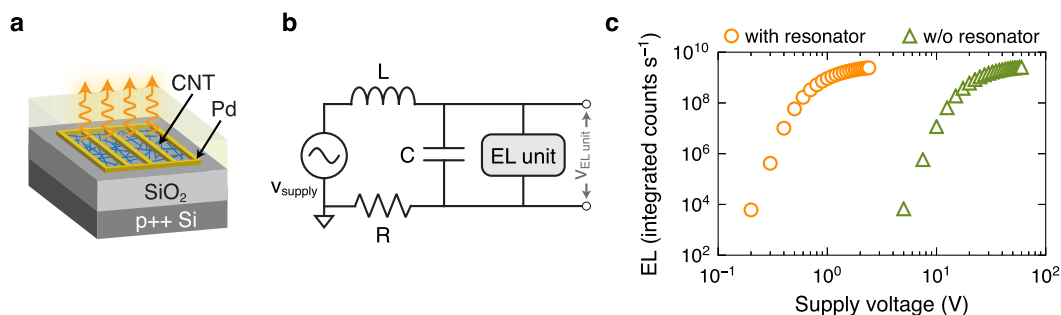


Figure 1. (a) Schematic of the device structure which consists of an emissive film deposited on top of a capacitor on a silicon substrate. The device is operated by applying an alternating current sinusoidal voltage across the two terminals of the capacitor. (b) Simplified diagram of the device operating scheme, where external reactive elements (L , C) are used to tune the operating frequency. (c) EL intensity as a function of voltage when the device is driven directly by an approximately 15 kHz sinusoidal voltage source (without a resonator, green triangles) or via the scheme depicted in (a) with $L = 100$ mH, $C = 1$ nF (with a resonator, orange circles).

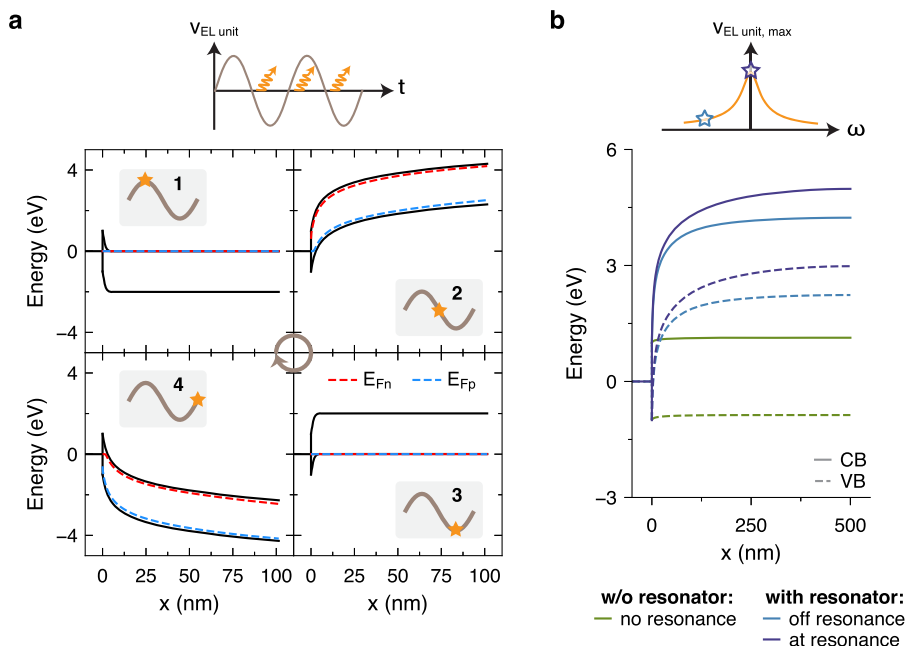


Figure 2. (a) Simulated energy band diagrams at the interface between a metallic CNT contact and a semiconducting emissive material at different time points of a sine wave excitation. Dashed red and blue lines represent the quasi-Fermi levels for electrons and holes, respectively. (b) Conduction (solid lines) and valence (dashed lines) bands corresponding to time point 2 for a device operated in a resonant driving scheme at the resonance frequency (purple lines, corresponding to (a)) and 1 kHz away from the resonance frequency (blue lines) with a supply voltage of 1 V. Band bending is nearly absent when driven nonresonantly (green lines), leading to substantially less quasi-Fermi level splitting (not shown). The driving scheme illustrated in Figure 1b,c, and the assembled CNT network is assumed to be lossless.

molecular materials using the same structure due to poor lateral carrier transport. By use of a CNT network as the top source contact, large-area emission can be obtained from materials with low or imbalanced charge carrier mobility, such as organic thin films. Previous work elucidates the critical role of the CNT network in such a device: the density of the CNT network must be high enough for electrical percolation across a large area but not so high that it hinders gate control of the semiconducting layer.¹¹ These devices, while versatile, suffer from low efficiencies in the range of less than 1% which hinders their practical utility, and it remains unknown whether reasonable operating efficiency can be attained using such a scheme. Furthermore, bright electroluminescence typically requires either thin gate oxide layers or high drive voltages. Reducing the gate oxide thickness to the several nanometer range requires tight fabrication tolerances and limits the

operating voltage range, while high drive voltages require high voltage electronics that impose bandwidth constraints and increase the system size.

Similar top-emitting AC electroluminescent devices based on MOS transistors (e.g., light-emitting field-effect transistors) have been previously developed, but the power efficiencies are unreported or low (on the order of $<10^{-5}$ lm/W^{13–16}). Here, we show that high power efficiencies can be achieved with AC-driven MOS capacitor devices by using a bright, vacuum deposited, organic emissive layer. We further analyze AC electrical characteristics of the device through impedance spectroscopy and demonstrate how devices with different gate oxide thicknesses can be driven with low supply voltages, simply by operating the device in a resonant LC tank circuit with reactive components that match the impedance of the device (Figure 1b,c). By combining these strategies, we

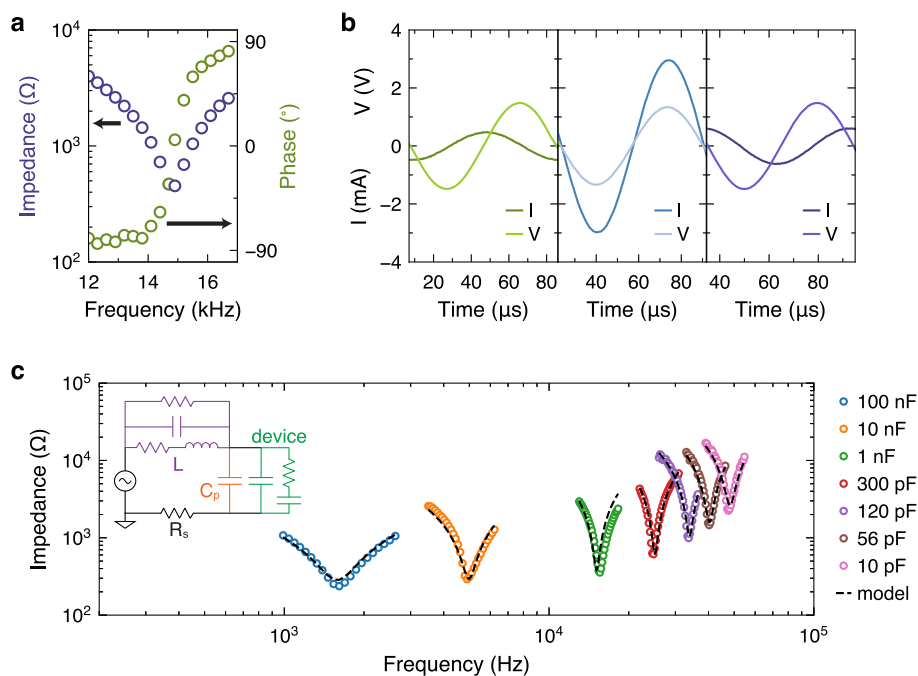


Figure 3. (a) Impedance and phase between the current–voltage waveforms near the resonance frequency measured using the scheme depicted in Figure 1b. (b) From left to right: current and voltage seen at the source below, at, and above the resonance frequency. The amplitude of the voltage source is 1.5 V. (c) Impedance of LC tank circuits with a 100 mH inductor and the base device structure in parallel with different capacitors (inset: model of the resonant circuit). Refer to Supporting Information for more information.

demonstrate an AC-driven electroluminescent device with a power efficiency of >20 lm/W at a luminance of >1000 cd/m² when driven by a 0.7 V input RMS voltage.

RESULTS AND DISCUSSION

The structure of the AC electroluminescent device is shown in Figure 1a and the fabrication procedure is depicted in Supporting Information Figure S1. A solution-processed CNT network (Supporting Information Figure S2) serves as the top electrode, and a p++ Si/SiO₂ substrate serves as the bottom electrode and dielectric layer. An emissive layer is deposited directly on top of this capacitive structure, and EL is generated upon application of a sinusoidal AC voltage between the top and bottom electrodes. The CNT network serves as a dense but porous source contact¹⁷ and enables greater emission intensity from low mobility molecular materials while still allowing the transverse gate field to modulate the contact–semiconductor interface. We used metallic as opposed to semiconducting CNT networks¹⁸ in order to reduce resistive losses in the source contacts and produce devices with relatively linear electrical response in above-threshold AC operation (Supporting Information Figure S3). The operating mechanism of the device has been discussed previously and is supported by simulations which show how both electrons and holes can be injected into the emissive layer¹² (Figure 2a). At the positive peak of the applied sine wave voltage, electrons are accumulated in the emissive semiconducting material. As the gate voltage changes from positive to negative, the bands of the semiconducting material near the CNT source contact bend upward, causing holes to tunnel into the emissive semiconducting material while electrons exit. The temporary presence of both charge carriers permits subsequent exciton formation and radiative recombination leading to light emission (Supporting Information

Figure S4). As the gate voltage reaches its peak negative value, the semiconducting material now largely contains only holes, and a similar carrier injection process occurs at the negative-to-positive voltage transition.

In this operating scheme, high input voltages are required to generate band bending steep enough to enable sufficient carrier tunneling. However, due to the AC mode of device operation, the capacitive electroluminescent device can be operated resonantly such that bright emission is achieved at low supply voltages. By addition of reactive electronic components to the driving scheme that cancel the capacitive reactance of the device, the supply voltage can be entirely dropped across the lossy resistive components of the circuit at resonance, which include the source contact (paths along the CNT network) and process of carrier injection from the contact to the emissive layer (Figure 2b). During this process, voltage is dropped at the contact–semiconductor interface and within the semiconductor, but the former dominates. At the same time, the peak voltage across the gate oxide is magnified, further enhancing the band bending at the metal–semiconductor interface as energy sloshes between the capacitive and inductive elements. For instance, when an inductor is added in series with the capacitive device, electrical resonance is achieved at the frequency where the impedance of the inductor ($Z_L = j\omega L$) matches the impedance of the capacitive component of the device ($Z_C = 1/(j\omega C_{\text{device}})$). At the resonance point of this tuned resistor–inductor–capacitor (RLC) resonator (i.e., at $\omega_0 = 1/\sqrt{LC_{\text{device}}}$), the reactive impedances of the inductor and capacitor cancel out and the total impedance only reflects resistive components of the impedance of the components.¹⁹ The resonance frequency can be additionally tuned by adding more reactive elements to the driving scheme such as a capacitor C_p in parallel with the device.

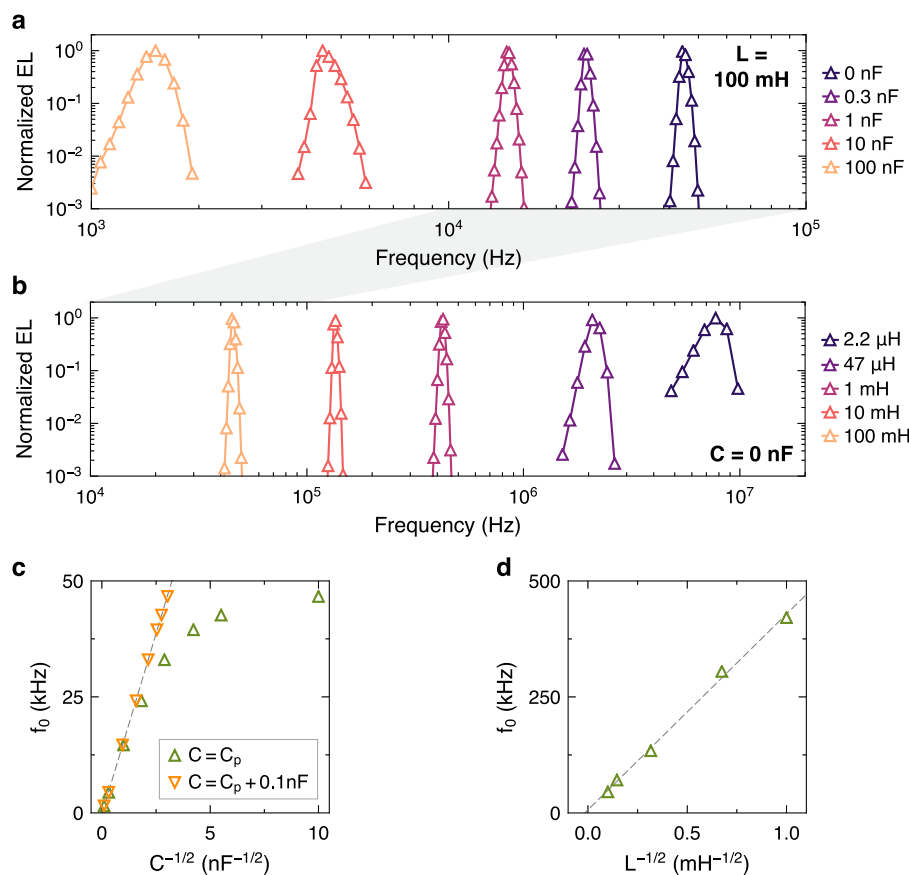


Figure 4. (a) Normalized EL intensity as a function of frequency for resonantly operated AC electroluminescent devices using (a) a 100 mH inductor and varying parallel capacitances C_p indicated in the legend or (b) no parallel capacitance and varying series inductances L indicated in the legend. (c) Resonance frequency as a function of \sqrt{C} for the data in (a) where C represents the external capacitance alone (upward triangles) or in sum with a fitted value (downward triangles). (d) Resonance frequency as a function of L for the data in (b). Dashed lines represent least-squares linear fits.

Impedance data show that the device largely behaves as a capacitor with a capacitance around 55 pF, which is consistent with the geometry of the device; the metal grid has a ~ 30 pF capacitance on SiO₂ with $\epsilon = 3.9\epsilon_0$, in addition to extra capacitance arising from the metallic CNT network covering a fraction of the emission area. When the device is connected in parallel with a 1 nF capacitor and in series with a 100 mH inductor, electrical resonance is achieved at the frequency where the impedance dips to a minimum and the phase shifts from -90° (mostly capacitive) to $+90^\circ$ (mostly inductive), as shown in Figure 3a. In this case, the resonance frequency is mostly determined by L and C_p since $C_p \gg C_{\text{device}}$. Due to the decrease in total impedance, the maximum source current is magnified as well, yielding higher carrier injection at a lower supply voltage (Figure 3b). The reduction in supply voltage depends on the Q -factor of the circuit, which is given by

$$Q = \frac{\omega_0 L}{R} = \frac{1}{R} \sqrt{\frac{L}{C}}$$

and is around 25 in this case. The Q -factor can be increased by decreasing parasitic resistance in the device and setup, as well as by maximizing the L/C ratio. Figure 3c shows a more complete equivalent circuit model of the resonant circuit which characterizes frequency-dependent impedance data of the device operated at different resonance frequencies using different component choices; detailed discussion of the

resonant circuit model and Q -factor optimization can be found in Supplementary Notes 1 and 2.

The resonance frequency can be tuned by choosing suitable values of externally added reactive components in conjunction with the device impedance. To demonstrate the electrical tunability of the operating scheme, we used devices with a drop-casted emissive layer of Ir(dtb-bpy)(ppy)₂PF₆ due to its ease of fabrication, low volumes of material required, and relatively bright single-layer emission even when processed under ambient conditions.²⁰ Figure 4a and Figure 4b show how the resonance frequency changes when the parallel capacitance or series inductance are varied, respectively. As the parallel capacitance or series inductance increases, the resonance frequency decreases. The resonance frequency ranges from 1 to 2 kHz at the largest LC value used to 8–9 MHz at the smallest LC value used, which represents a span of 4 orders of magnitude. Broad frequency-dependent measurements also enable quantification of the resonance frequency, which should scale linearly with \sqrt{LC} as Figure 3d shows for varying inductance values. The equivalent circuit capacitance can be alternatively extracted by finding the value of C_{eq} that yields the closest straight-line relationship between the resonance frequency and $\sqrt{C} = \sqrt{C_p + C_{\text{eq}}}$ (for known C_p) as shown in Figure 4c. In both cases, the measured device has an equivalent capacitance of around 0.1 nF. It should be noted that the behavior of resonant circuits depends on stray

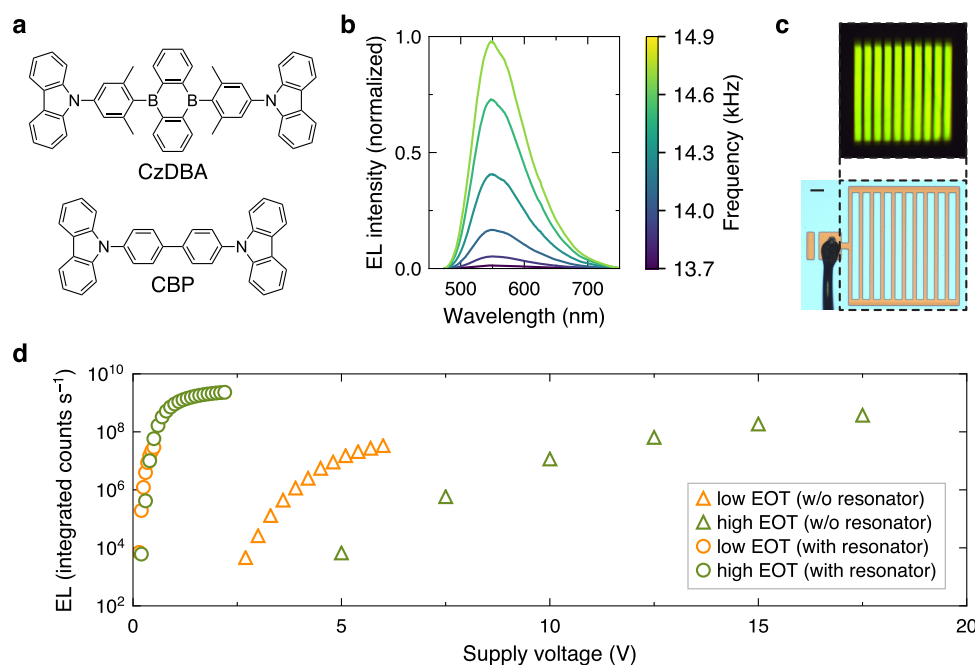


Figure 5. (a) Molecular structures of the dopant (CzDBA) and host (CBP) coevaporated as the emissive layer of the device. (b) EL spectra for different frequencies near the resonance frequency, with the voltage across the device increasing toward 15 kHz. The device is driven by a 0.7 V_{rms} source voltage using $L = 100$ mH, $C_p = 1$ nF. (c) Optical image of the device and visible green emission from the emission area between the metal grid lines. Scale bar is 50 μ m. (d) EL intensity as a function of supply voltage for devices with low (≈ 4 nm) and high (≈ 90 nm) equivalent oxide thickness driven without and with the resonator at the resonance frequency.

parasitics and nonidealities in the discrete components, which have been disregarded so far for simplicity. These complexities, such as self-resonance in the inductor, are elaborated in [Supplementary Note 1](#).

Previous work on MOS capacitor-based AC electro-luminescent devices showed dim brightness levels on the order of 10^2 cd/m² and low external quantum efficiencies in the range of a few percent or less, with power efficiencies lagging even further behind.¹¹ The external efficiency of a light emitting device depends fundamentally on the internal efficiency of the emissive material. Conventional fluorescent materials are limited by spin statistics and can only achieve 25% internal efficiency at best due to nonradiative triplet transitions. To address this problem, highly efficient next generation phosphorescent and thermally activated delayed fluorescence (TADF) emitters have been developed.^{21–23} To demonstrate the performance limits of the presented device and operating scheme, we fabricated devices with a ~ 30 nm, thermally evaporated emissive layer consisting of the TADF emitter CzDBA doped in the host material CBP^{24,25} (Figure 5a). The emission spectrum redshifts with increasing dopant concentration, and a moderate (~ 16 wt %) dopant to host concentration was found to yield brighter EL in general ([Supporting Information Figure S5](#)). The EL spectra for this emissive layer show a peak EL intensity around 550 nm with bright yellow-green emission in between the metal grid lines where the underlying CNT networks have been patterned (Figure 5b,c). Frequency-dependent measurements of EL generated from this material show monotonically increasing EL intensity with increasing sine wave frequency ([Supporting Information Figure S6](#)), which is expected since there are more voltage polarity transitions per second at higher frequencies. When the EL intensity is normalized by frequency, there is a frequency (on the order of 10 kHz) at which peak EL per sine

wave cycle is achieved. Below this frequency, the EL intensity per cycle decreases with decreasing frequency due to the increasingly sluggish voltage transitions which produce less sharp band bending. Above this frequency, the EL intensity per cycle decreases due to the slow electro-luminescent response of the device, which depends on both the RC time constant and the intrinsic photoluminescence lifetime.

On the basis of the frequency-dependent EL and earlier Q-factor results ([Supplementary Note 2](#)), we characterized the device at an operating frequency around 15 kHz. The resonant driving scheme can be applied at this frequency by choosing a series inductance of 100 mH and a parallel capacitance of 1 nF, which yields a Q-factor of around 25. Voltage-dependent measurements of the device operating at this frequency show that EL is generated at much lower supply voltages when driven resonantly as opposed to nonresonantly (Figure 5d). As established previously,²⁶ the turn-on voltage for electro-luminescence can be fundamentally reduced by decreasing the equivalent gate oxide thickness to the several nanometers range; however, this imposes constraints on the precision of the fabrication process. Absent the resonant driving scheme, the turn-on voltage is reduced by half by using a device with a thinner, high- k gate dielectric layer. However, by driving the device resonantly, the turn-on voltage of the device (as defined at the source) is reduced to the millivolt range for devices with different equivalent gate oxide thicknesses. EL can be observed at around 0.25 V for a device with either a thin high- k gate dielectric or a thicker low- k gate dielectric, meaning that the resonant driving scheme enables EL at low turn-on voltages for a wide range of gate oxide thicknesses. Reducing the sensitivity of the turn-on voltage to gate oxide thickness is attractive from a design and fabrication perspective, as it eases the requirement for thin, precisely fabricated gate oxide layers.

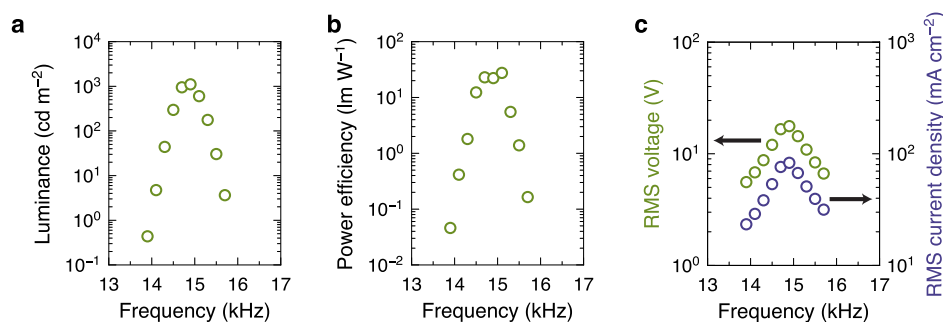


Figure 6. (a) Luminance, (b) power efficiency, and (c) RMS voltage and current density as a function of frequency for a device driven by a 0.7 V_{rms} source voltage using $L = 100$ mH, $C_p = 1$ nF with a CzDBA/CBP emissive layer.

Finally, we characterized the brightness and power efficiency of the resonantly driven electroluminescent device. Under an AC driving scheme, the average real power consumed by the device can be calculated as

$$\frac{1}{T} \int_0^T I(t)V(t) dt$$

where $I(t)$ and $V(t)$ are the current and voltage across the device, respectively.²⁷ For sinusoidal modulation, the real dissipated power simplifies as $I_{\text{rms}}V_{\text{rms}} \cos(\theta)$ where $\cos(\theta)$ is the phase shift or power factor that determines the loss. Alternatively, the power consumption at resonance can be interpreted from the Q -factor, which relates to the ratio of energy stored to energy lost per cycle (Supplementary Note 3). Using this operating scheme, a peak EL brightness of 1108 cd/m^2 is observed for a device driven by a 0.7 V_{rms} , 14.9 kHz sinusoidal input (Figure 6). In this luminance range, the power efficiency generally increases in the vicinity of the resonance frequency, with a peak power efficiency of 28 lm/W . The EL intensity increases near resonance as the current through the device increases and more charge is injected. The spectral shape or color is invariant to the applied frequency and voltage (Supporting Information Figure S7). Voltage-dependent EL measurements of a device operated at the resonance frequency show that the power efficiency increases with voltage near the turn-on regime (~ 1 V) but steadily decreases thereafter (Supporting Information Figure S8), as the increase in luminance fails to keep pace with the increase in power consumption. The efficiency of organic electroluminescent devices typically exhibits a roll-off at high current densities or brightness levels due to a combination of exciton loss mechanisms such as triplet–triplet annihilation and field-induced quenching.²⁸ These effects may be exaggerated in AC electroluminescent devices where charge carriers are injected one polarity at a time in alternating pulses with high energies and concentrations near the contact depending on the degree of band bending. Although the net power consumption of AC-driven devices is lower than equivalently driven DC devices due to the largely nondissipative charging and discharging-based operation, the peak current densities into the semiconducting layer can still be high. Furthermore, temporal simulations of the device's operating mechanism suggest that pulsed carrier injection is less efficient above a certain threshold voltage, since returning carriers are swept out through the source contact more rapidly and are less likely to recombine with incoming injected carriers of the opposite polarity.²⁶ Finally, heating effects may play a role in degraded device behavior.

The maximal performance values are overall considerably higher than those for the same device structure previously reported (around ~ 0.1 lm/W power efficiency at 10 cd/m^2 for a similar driving waveform and frequency¹¹) and rival the highest values reported for AC electroluminescent devices, which typically show relatively poor power efficiencies.^{11,29} A variety of other capacitive AC electroluminescent devices based on insulating and organic emissive layers have been developed, but these devices either have low power efficiencies (below 1 lm/W ^{30,31}) or require complex multilayered structures to reach comparable power efficiency.³² Supplementary Table 1 presents a comparison of the power efficiency of the device in this paper with related technologies. While the performance of the presented device still lags that of DC-driven LEDs based on the same emissive materials, the results show that relatively bright and efficient light-emitting devices can still be achieved with a concise device structure that requires only one active semiconducting layer and no additional layers specifically engineered for the emissive material. The simplified device architecture allows for pin-hole-tolerant fabrication of the active organic layer since thickness variations and particles on the substrate do not create detrimental electrical shunt paths.³³ From an electrical standpoint, the limit of device efficiency in this scheme ultimately depends on dissipative processes intrinsic to the device; such losses can be revealed by resonant measurements as described in this work. To improve efficiency of the methodology, external resistance in the source contact (i.e., the loss measured before the electroluminescent layer is deposited) and external circuitry should be minimized such that losses at or in the semiconductor dominate. On the basis of the impedance observed at resonance for the base device structure with and without the emissive layer (Figure 3), the effective resistance during AC operation increases by around 2 times when the luminescent material is deposited. Thus, the efficiency and effectiveness of the driving scheme could be up to twice as high in this case if the losses extrinsic to the EL process were to be theoretically eliminated.

CONCLUSION

In summary, we have demonstrated how reactive components can be designed to generate passive voltage gain across capacitive AC electroluminescent devices via a resonant tank circuit with high Q -factor. This simple operating scheme enables AC electroluminescent devices to be driven at low input voltages in a variety of applications and circumvents the need for additional active electronics which have limited gain-bandwidth product at high operating frequencies, an important

consideration for high-speed light-emitting devices. The insensitivity of the operating scheme to the thickness of the dielectric and emissive layers suggests that electroluminescent MOS capacitor devices, alongside properly engineered on-chip inductors, may be amenable to large-scale fabrication via solution-based printing methods, although the efficiency of this methodology depends critically on parasitic but typically unavoidable losses in the external inductive components. By selection of a bright and high-quality emissive layer, luminance levels (on the order of 10^3 cd/m²) and power efficiencies (on the order of tens of lm/W) are achieved, which are over an order of magnitude higher than the values previously measured for the same device structure and approach the values for conventional, direct current-driven organic light-emitting diodes. Thus, relatively high power efficiencies can be attained even with just a single generic contact for bipolar injection and it may be possible to construct viable light-emitting MOS capacitors at other wavelengths for practical light-emitting device applications in the future.

METHODS

Device Fabrication. The fabrication of solution-processed CNT networks has been previously described.³⁴ Devices were fabricated on 90 nm SiO₂ since the light outcoupling factor due to optical interference from the substrate stack is relatively higher with this gate oxide thickness at the wavelengths of interest.³⁵ 90 nm SiO₂/p++ Si substrates underwent O₂ plasma treatment for 1.5 min, followed by immersion in poly L-lysine solution (0.1% w/v aqueous solution, Ted Pella) for 5 min and rinsing with deionized (DI) water. Next, 90% metallic CNT solution (1 mg M90% IsoNanotubes-M, NanoIntegris) was drop-casted on the substrate at 100 °C, then rinsed with DI water after the solution dried. The substrate was annealed in forming gas for 1 h at 250 °C. Metal bond pads were patterned by photolithography with positive resist (LOR 5A/S1818) using a laser writer (Heidelberg μ PG 101) and deposited by e-beam evaporation of 0.5 nm Ti/25 nm Pd, followed by liftoff in PG remover at 70 °C. To reduce leakage current, the emission area for each device was defined by a second photolithography step and CNTs outside the device areas were etched by O₂ plasma. For the solution-processed emissive layer, a 10 mg/mL solution of Ir(dtbbpy)(ppy)₂ ([4,4'-bis(1,1-dimethylethyl)-2,2'-bipyridine-N1,N1']bis[2-(2-pyridinyl-N)phenyl-C]iridium(III) hexafluorophosphate, Sigma-Aldrich) in acetonitrile was prepared under ambient conditions and drop-casted on top of the device at 60 °C to promote solvent evaporation and uniform film formation. For the thermally evaporated emissive layer, a 16 wt % dopant:host film was co-deposited on top of the device at a base pressure below 2×10^{-6} Torr, where the dopant is CzDBA (5,10-bis(4-(9H-carbazol-9-yl)-2,6-dimethylphenyl)-5,10-dihydroboranthrene, $\geq 99\%$, Luminescence Technology) and the host is CBP (4,4'-bis(N-carbazolyl)-1,1'-biphenyl, $\geq 99.5\%$, Ossila).

Device Characterization. AC voltages were applied with a function generator (Agilent 33522A). Optical measurements were performed in vacuum (~ 20 mTorr) with a custom micro-PL instrument in which EL is dispersed by a spectrometer and detected with a charge-coupled device (CCD) (Andor iDus BEX2-DD). The emission power was measured with a power meter (Thorlabs PM100D with S120C photodiode sensor) and cross-calibrated with CCD counts. AC electrical measurements were performed simultaneously with an oscilloscope (Tektronix TDS 640A), and electrical current was measured with a shunt resistor or a current preamplifier (Stanford Research Systems SR570) where necessary. Component measurements and impedance values were cross-checked with an LCR meter (Agilent E4980AL). DC electrical measurements were performed with a semiconductor parameter analyzer (Agilent 4155C). The external power efficiency was determined by dividing the emission power by the electrical power consumption, which is

calculated by integrating the current–voltage product over one period of the sinusoid.

Device Simulation. Two-dimensional device simulations were performed using Sentaurus TCAD (Synopsys) as previously described.¹² The simulated device consisted of a layer of emissive semiconducting material situated on top of a 90 nm SiO₂ gate oxide layer with relative permittivity $\epsilon = 3.9$. Two 1.4 nm tall contacts representing neighboring CNTs were placed on each lateral end of the emissive semiconducting material. A sinusoidal AC voltage was applied between the CNT source contacts and a bottom gate electrode underneath the gate oxide. The CNT–CNT spacing was 1 μ m, and the work function of the CNT contacts was set to be mid-gap relative to the bandgap of the semiconducting material in order to generate ambipolar behavior. Material parameters were E_g (bandgap) = 2 eV, ϵ (relative permittivity) = 3.5, m_e^* (electron effective mass) = m_h^* (hole effective mass) = m_0 , and μ_n (electron mobility) = μ_p (hole mobility) = 0.001 cm² V⁻¹ s⁻¹ for the semiconducting layer.³⁶ Carrier tunneling is enabled at the interface between the source contacts and semiconducting layer. The simulation, which provides a simplified view of device operation for illustrative purposes, assumes a free carrier model with entirely radiative recombination.

ASSOCIATED CONTENT

Supporting Information

The Supporting Information is available free of charge at <https://pubs.acs.org/doi/10.1021/acsnano.1c05729>.

Fabrication process; AC electrical characterization; simulation details; effect of emissive layer doping concentration; frequency- and voltage-dependent electroluminescence; equivalent circuit model; further discussion of RLC circuit operation, Q-factor, and power consumption (PDF)

AUTHOR INFORMATION

Corresponding Author

Ali Javey – *Electrical Engineering and Computer Sciences, University of California at Berkeley, Berkeley, California 94720, United States; Materials Sciences Division, Lawrence Berkeley National Laboratory, Berkeley, California 94720, United States; orcid.org/0000-0001-7214-7931; Email: ajavey@eecs.berkeley.edu*

Author

Vivian Wang – *Electrical Engineering and Computer Sciences, University of California at Berkeley, Berkeley, California 94720, United States; Materials Sciences Division, Lawrence Berkeley National Laboratory, Berkeley, California 94720, United States; orcid.org/0000-0001-8675-0782*

Complete contact information is available at: <https://pubs.acs.org/doi/10.1021/acsnano.1c05729>

Notes

The authors declare no competing financial interest.

ACKNOWLEDGMENTS

Materials characterization and processing were supported by the Electronic Materials Program, funded by U.S. Department of Energy, Office of Science, Office of Basic Energy Sciences, Materials Sciences and Engineering Division under Contract DE-AC02-05Ch11231. Device processing was supported by Samsung. The authors thank S. Z. Uddin for helpful discussions and W. Ji for aid with preliminary device fabrication. V.W. acknowledges support from the NSF Graduate Research Fellowship under Grant DGE-1752814.

REFERENCES

- (1) Dupuis, R. D.; Krames, M. R. History, Development, and Applications of High-Brightness Visible Light-Emitting Diodes. *J. Lightwave Technol.* **2008**, *26* (9), 1154–1171.
- (2) Destriau, G. Recherches Sur Les Scintillations Des Sulfures de Zinc Aux Rayons α . *J. Chim. Phys. Phys.-Chim. Biol.* **1936**, *33*, 587–625.
- (3) Adafruit. Adafruit Learning System: EL Wire <https://learn.adafruit.com/el-wire>.
- (4) Shi, X.; Zuo, Y.; Zhai, P.; Shen, J.; Yang, Y.; Gao, Z.; Liao, M.; Wu, J.; Wang, J.; Xu, X.; Tong, Q.; Zhang, B.; Wang, B.; Sun, X.; Zhang, L.; Pei, Q.; Jin, D.; Chen, P.; Peng, H. Large-Area Display Textiles Integrated with Functional Systems. *Nature* **2021**, *591* (7849), 240–245.
- (5) Hanton, O.; Wessely, M.; Mueller, S.; Fraser, M.; Roudaut, A. ProtoSpray: Combining 3D Printing and Spraying to Create Interactive Displays with Arbitrary Shapes. *Proceedings of the 2020 CHI Conference on Human Factors in Computing Systems* **2020**, 1–13.
- (6) Bernanose, A. Electroluminescence of Organic Compounds. *Br. J. Appl. Phys.* **1955**, *6* (S4), S54.
- (7) Adachi, C.; Baldo, M. A.; Thompson, M. E.; Forrest, S. R. Nearly 100% Internal Phosphorescence Efficiency in an Organic Light Emitting Device. *J. Appl. Phys.* **2001**, *90* (10), 5048–5051.
- (8) Reineke, S.; Lindner, F.; Schwartz, G.; Seidler, N.; Walzer, K.; Lüssem, B.; Leo, K. White Organic Light-Emitting Diodes with Fluorescent Tube Efficiency. *Nature* **2009**, *459* (7244), 234–238.
- (9) Gessmann, T.; Schubert, E. F. High-Efficiency AlGaInP Light-Emitting Diodes for Solid-State Lighting Applications. *J. Appl. Phys.* **2004**, *95* (5), 2203–2216.
- (10) Mitschke, U.; Bäuerle, P. The Electroluminescence of Organic Materials. *J. Mater. Chem.* **2000**, *10* (7), 1471–1507.
- (11) Zhao, Y.; Wang, V.; Lien, D. H.; Javey, A. A Generic Electroluminescent Device for Emission from Infrared to Ultraviolet Wavelengths. *Nat. Electron.* **2020**, *3* (10), 612–621.
- (12) Lien, D. H.; Amani, M.; Desai, S. B.; Ahn, G. H.; Han, K.; He, J. H.; Ager, J. W.; Wu, M. C.; Javey, A. Large-Area and Bright Pulsed Electroluminescence in Monolayer Semiconductors. *Nat. Commun.* **2018**, *9* (1), 1–7.
- (13) Maddalena, F.; Chin, X. Y.; Cortecchia, D.; Bruno, A.; Soci, C. Brightness Enhancement in Pulsed-Operated Perovskite Light-Emitting Transistors. *ACS Appl. Mater. Interfaces* **2018**, *10* (43), 37316–37325.
- (14) Yamao, T.; Shimizu, Y.; Terasaki, K.; Hotta, S. Organic Light-Emitting Field-Effect Transistors Operated by Alternating-Current Gate Voltages. *Adv. Mater.* **2008**, *20* (21), 4109–4112.
- (15) Kajiwara, K.; Terasaki, K.; Yamao, T.; Hotta, S. Light-Emitting Field-Effect Transistors Consisting of Bilayer-Crystal Organic Semiconductors. *Adv. Funct. Mater.* **2011**, *21* (15), 2854–2860.
- (16) Marconi, A.; Anopchenko, A.; Pucker, G.; Pavesi, L. Power Efficiency Estimation of Silicon Nanocrystals Based Light Emitting Devices in Alternating Current Regime. *Appl. Phys. Lett.* **2011**, *98* (20), 201103.
- (17) Hecht, D. S.; Hu, L.; Irvin, G. Emerging Transparent Electrodes Based on Thin Films of Carbon Nanotubes, Graphene, and Metallic Nanostructures. *Adv. Mater.* **2011**, *23* (13), 1482–1513.
- (18) Topinka, M. A.; Rowell, M. W.; Goldhaber-Gordon, D.; McGehee, M. D.; Hecht, D. S.; Gruner, G. Charge Transport in Interpenetrating Networks of Semiconducting and Metallic Carbon Nanotubes. *Nano Lett.* **2009**, *9* (5), 1866–1871.
- (19) Bowick, C.; Blyler, J.; Ajluni, C. *RF Circuit Design*, 2nd ed.; Newnes: Burlington, MA, 2008.
- (20) Slinker, J. D.; Gorodetsky, A. A.; Lowry, M. S.; Wang, J.; Parker, S.; Rohl, R.; Bernhard, S.; Malliaras, G. G. Efficient Yellow Electroluminescence from a Single Layer of a Cyclometalated Iridium Complex. *J. Am. Chem. Soc.* **2004**, *126* (9), 2763–2767.
- (21) Ràfols-Ribé, J.; Will, P. A.; Hänisch, C.; Gonzalez-Silveira, M.; Lenk, S.; Rodríguez-Viejo, J.; Reineke, S. High-Performance Organic Light-Emitting Diodes Comprising Ultrastable Glass Layers. *Sci. Adv.* **2018**, *4* (5), eaar8332.
- (22) Goushi, K.; Yoshida, K.; Sato, K.; Adachi, C. Organic Light-Emitting Diodes Employing Efficient Reverse Intersystem Crossing for Triplet-to-Singlet State Conversion. *Nat. Photonics* **2012**, *6* (4), 253–258.
- (23) Uoyama, H.; Goushi, K.; Shizu, K.; Nomura, H.; Adachi, C. Highly Efficient Organic Light-Emitting Diodes from Delayed Fluorescence. *Nature* **2012**, *492* (7428), 234–238.
- (24) Wu, T. L.; Huang, M. J.; Lin, C. C.; Huang, P. Y.; Chou, T. Y.; Chen-Cheng, R. W.; Lin, H. W.; Liu, R. S.; Cheng, C. H. Diboron Compound-Based Organic Light-Emitting Diodes with High Efficiency and Reduced Efficiency Roll-Off. *Nat. Photonics* **2018**, *12* (4), 235–240.
- (25) Kotadiya, N. B.; Blom, P. W. M.; Wetzelaer, G. J. A. H. Efficient and Stable Single-Layer Organic Light-Emitting Diodes Based on Thermally Activated Delayed Fluorescence. *Nat. Photonics* **2019**, *13* (11), 765–769.
- (26) Wang, V.; Zhao, Y.; Javey, A. Performance Limits of an Alternating Current Electroluminescent Device. *Adv. Mater.* **2021**, *33* (2), 2005635.
- (27) Chen, Y.; Xia, Y.; Smith, G. M.; Carroll, D. L. Frequency-Dependent, Alternating Current-Driven, Field-Induced Polymer Electroluminescent Devices with High Power Efficiency. *Adv. Mater.* **2014**, *26* (48), 8133–8140.
- (28) Murawski, C.; Leo, K.; Gather, M. C. Efficiency Roll-Off in Organic Light-Emitting Diodes. *Adv. Mater.* **2013**, *25* (47), 6801–6827.
- (29) Wang, L.; Xiao, L.; Gu, H.; Sun, H. Advances in Alternating Current Electroluminescent Devices. *Adv. Opt. Mater.* **2019**, *7* (7), 1801154.
- (30) Cho, S. H.; Jo, S. S.; Hwang, I.; Sung, J.; Seo, J.; Jung, S. H.; Bae, I.; Choi, J. R.; Cho, H.; Lee, T.; Lee, J. K.; Lee, T. W.; Park, C. Extremely Bright Full Color Alternating Current Electroluminescence of Solution-Blended Fluorescent Polymers with Self-Assembled Block Copolymer Micelles. *ACS Nano* **2013**, *7* (12), 10809–10817.
- (31) Perumal, A.; Lüssem, B.; Leo, K. High Brightness Alternating Current Electroluminescence with Organic Light Emitting Material. *Appl. Phys. Lett.* **2012**, *100* (10), 103307.
- (32) Chen, Y.; Xia, Y.; Smith, G. M.; Sun, H.; Yang, D.; Ma, D.; Li, Y.; Huang, W.; Carroll, D. L. Solution-Processable Hole-Generation Layer and Electron-Transporting Layer: Towards High-Performance, Alternating-Current-Driven, Field-Induced Polymer Electroluminescent Devices. *Adv. Funct. Mater.* **2014**, *24* (18), 2677–2688.
- (33) Matsushima, T.; Bencheikh, F.; Komino, T.; Leyden, M. R.; Sandanayaka, A. S. D.; Qin, C.; Adachi, C. High Performance from Extraordinarily Thick Organic Light-Emitting Diodes. *Nature* **2019**, *572* (7770), 502–506.
- (34) Wang, C.; Hwang, D.; Yu, Z.; Takei, K.; Park, J.; Chen, T.; Ma, B.; Javey, A. User-Interactive Electronic Skin for Instantaneous Pressure Visualization. *Nat. Mater.* **2013**, *12* (10), 899–904.
- (35) Lien, D. H.; Kang, J. S.; Amani, M.; Chen, K.; Tosun, M.; Wang, H. P.; Roy, T.; Eggleston, M. S.; Wu, M. C.; Dubey, M.; Lee, S. C.; He, J. H.; Javey, A. Engineering Light Outcoupling in 2D Materials. *Nano Lett.* **2015**, *15* (2), 1356–1361.
- (36) Sanderson, S.; Philippa, B.; Vamvounis, G.; Burn, P. L.; White, R. D. Understanding Charge Transport in Ir(ppy)₃:CBP OLED Films. *J. Chem. Phys.* **2019**, *150*, 094110.